[9] C. M. Butler, "The equivalent radius of a narrow conducting strip," *IEEE Trans Antennas Propagat*, vol. AP-30, pp. 755–758, July 1982.
[10] I. E. Rana and N. G Alexopoulos, "Current distribution and input impedance of dipoles," *IEEE Trans. Antennas Propagat.*, vol. AP-29, pp. 99–105, Jan. 1981.
[11] S. M. Sze, *Physics of Semiconductor Devices*, 2nd edition. New York: Wiley, 1981.
[12] H. Bassen, "RF/Microwave radiation measurement, risk assessment and control activities at the Bureau of Radiological Health," *IEEE Antennas Propagat Soc. Newsletter*, vol. 23, pp. 5–8, Apr. 1981

Dynamic Behavior of Pulsed-IMPATT Oscillators

R K. MAINS, G. I. HADDAD, D. BOWLING, AND M. AFENDYKIW

***Abstract*—A method of simulating the dynamic behavior of pulsed-IMPATT oscillators is presented. It is assumed that the simulation variables change slowly with respect to the RF period so that the quasi-static approximation may be used. A comparison of simulation results with experimental results for an *X*-band circuit is given.**

I. Introduction

The quasi-static approximation may be effectively used to simulate transient effects in free-running and injection-locked pulsed oscillators [1], [2]. It is an alternative to the time-consuming method of performing a complete device-circuit interaction simulation in the time domain using a small time step due to stability restrictions on the device simulation. The quasi-static method requires a complete steady-state characterization of the IMPATT device over the ranges of temperature, bias current density, and RF voltage amplitude that will be encountered in the transient simulation. It is then assumed that the simulation parameters change slowly with respect to the RF period so that the IMPATT appears to be in a steady-state condition at any particular instant of time. In this manner, the transient can readily be simulated over the entire pulse width.

II. IMPATT Device Model

Fig. 1 shows the doping profile of the GaAs double-drift IMPATT diode used in the simulations. This particular structure was fabricated by Microwave Associates, Inc., and was also used in the experimental phase of the investigation. This diode was simulated at 10 GHz using the computer programs developed by Bauhahn and Haddad [3], [4] and later modified by Mains and Haddad [5], wherein it is assumed that the particle currents consist of a drift plus diffusion term, with drift velocities and diffusion coefficients expressed as functions of the local electric field. Simulations were carried out at temperatures $T = 300$, 400, 500, 535, and 575° K. At each temperature, simulations were performed at bias current densities of $J_{dc} = 400$, 650, and 1000 A/cm^2. For each (T, J_{dc}) combination, a sinusoidal RF voltage at 10 GHz was applied and the amplitude was varied from zero to the point where the diode efficiency dropped significantly. The information thus obtained is Y_D $(f = 10$ GHz; $T, J_{dc}, V_{RF})$, the diode admittance in mho/cm^2, and V_{dc} $(f = 10$ GHz; $T, J_{dc}, V_{RF})$, the diode large-signal operating voltage. At $J_{dc} = 0$, the diode is modeled as a depletion capacitance $C_0 = (\epsilon A / w_d)F$ in series with a small resistor $R_0 = (w_u/\sigma A)\Omega$ to account for the undepleted region (w_d is the depletion region width and w_u is the width of the undepleted region). To obtain the diode characteristics at operating points other than those simulated, a linear interpolation scheme is used [2].

It is assumed that the circuit admittance $Y_c(s)$ varies more rapidly with frequency than the diode admittance so that Y_D may be assumed constant with frequency over the range of interest. However, the diode cold capacitance $C_D = (\epsilon / w)$ F/cm^2 (where $w = w_d + w_u = 6.95$ μm) is lumped into $Y_c(s)$ so that the ωC_D component of the diode susceptance does vary with frequency. The device area was assumed to be $A = 1.3 \times 10^{-3}$ cm^2, which is the measured value for the diode.

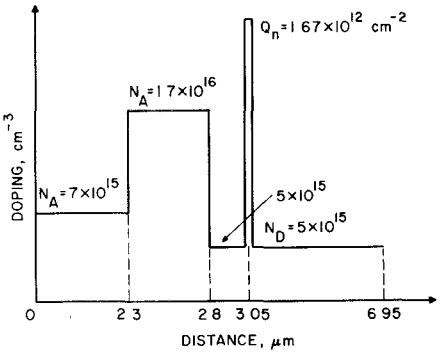

Fig. 1. Doping profile of GaAs IMPATT diode used in the theoretical and experimental investigations (diode area $A = 1.3 \times 10^{-3}$ cm^2).

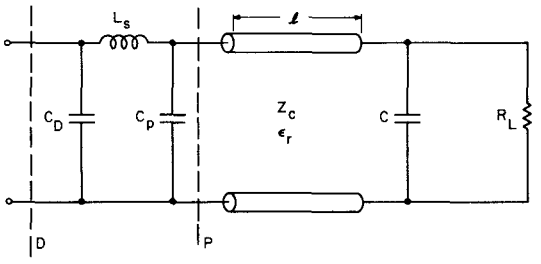

Fig. 2. Circuit model used for the simulations ($C_D = 2.07$ pF, $L_s = 0.153$ nH, $C_p = 0.32$ pF, $Z_c = 3.98$ Ω, $\epsilon_r = 2.53$, $l = 0.2667$ cm, $C = 0.111$ pF, and $R_L = 50$ Ω).

III. Circuit Model

Fig. 2 shows the circuit used to model the actual oscillator circuit, which consists of a 50-Ω transmission line (represented by R_L) and a low-impedance transformer adjacent to the diode package (represented by Z_c, l, and ϵ_r). The capacitance C is the discontinuity capacitance between the 50-Ω transmission line and the transformer. The circuit elements to the right of plane P were verified from experimental impedance measurements at this plane. It was attempted to measure the package-mounting equivalent circuit elements L_s and C_p; however some uncertainty remained concerning these values, especially for the series inductance L_s. The procedure was to use the experimentally determined value of 0.32 pF for C_p and to determine L_s as follows. The diode admittance resulting from the simulation at $T = 500$°K, $J_{dc} = 650$ A/cm^2 (the bias current density used experimentally) and $V_{RF} =$

Manuscript received June 29, 1983; revised October 7, 1983. This work was supported in part by the Naval Weapons Center, China Lake, CA

R. K. Mains and G. I. Haddad are with the Electron Physics Laboratory, Department of Electrical and Computer Engineering, University of Michigan, Ann Arbor

D. Bowling and M. Afendykiw are with the Naval Weapons Center, China Lake, CA 93555.

0018-9480/84/0200-0208$01.00 ©1984 IEEE

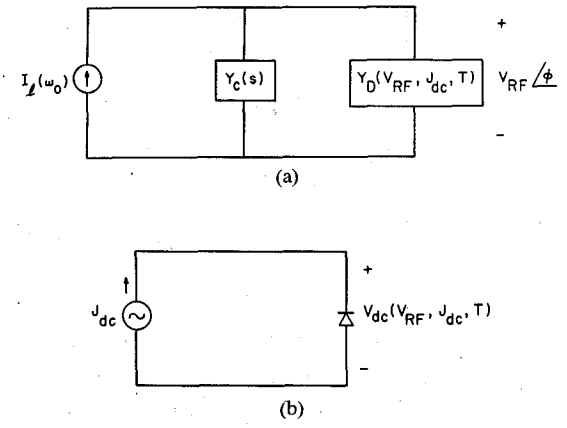

Fig. 3. (a) RF circuit and (b) bias circuit used in the simulation.

57.17 V (maximum efficiency point for this particular (T, J_{dc}) combination) was transformed through the package-mounting equivalent circuit to plane P in Fig. 2. L_s was then chosen so that this transformed admittance was equal to the experimental large-signal admittance measurements at plane P. C_D is the diode cold capacitance, which is lumped into the circuit model.

IV. Quasi-Static, Device-Circuit Interaction Simulation Procedure

Fig. 3 indicates the overall procedure used in the simulation. In Fig. 3(a), $Y_c(s)$ is the admittance versus complex frequency s of the circuit in Fig. 2 at plane D, $Y_D(V_{RF}, J_{dc}, T)$ is the diode admittance determined from the large-signal device simulation, $I_I(\omega_0)$ is the injection current used to simulate the injection-locked case, V_{RF} is the (peak) amplitude of the RF voltage at the diode terminals, and ϕ is the phase of this voltage relative to $I_I(\omega_0)$. Both V_{RF} and ϕ are slowly varying functions of time. The complex frequency s is obtained at each time step by solving the equation

$$Y_c(s)+Y_D(V_{RF}, J_{dc}, T)=\frac{I_L}{V_{RF}}e^{-j\phi}. \tag{1}$$

V_{RF} and ϕ are updated according to

$$\frac{1}{V_{RF}}\frac{dV_{RF}}{dt}=\sigma=\mathrm{Re}\{s\} \tag{2}$$

and

$$\frac{d\phi}{dt}=\omega-\omega_0=\mathrm{Im}\{s\}-\omega_0. \tag{3}$$

The diode temperature T is updated from

$$\frac{dT}{dt}=\frac{R_{th}P_D}{\tau}-\frac{T-T_A}{\tau} \tag{4}$$

where R_{th} is the diode thermal resistance in °K/W, P_D is the power dissipated in the diode in W, T_A is the ambient temperature in degrees Kelvin, and τ is the thermal relaxation time in seconds.

In Fig. 3(b), the bias current J_{dc} is assumed to rise linearly from zero to a constant value at turn on, to maintain this constant value throughout the pulse width, and then to fall linearly to zero at turn off. In principle, the bias circuit could be modeled and a second device-circuit interaction could be solved to determine the evolution of J_{dc} with time; however, this was not done in the simulations presented here.

For the injection-locked case, it is assumed that I_I is on long before the bias-current density J_{dc} is switched on at $t=0$. Therefore, at $t=0$ a substantial RF voltage exists across the diode terminals even though the device is passive at this time.

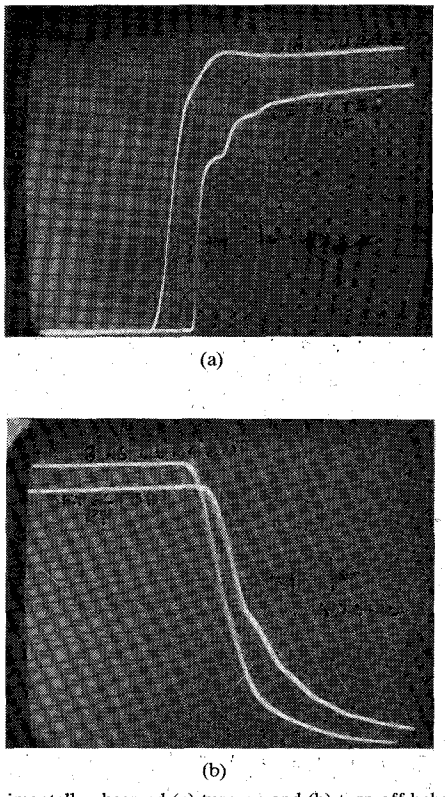

Fig. 4. Experimentally observed (a) turn-on and (b) turn-off behavior for the free-running case ($J_{dc}=646$ A/cm^2, pulse width $=1.5$ μs, and duty cycle $=45\%$).

V. Comparison of Theoretical and Experimental Results

Fig. 4 presents the turn-on and turn-off characteristics observed for the free-running case and Fig. 5(a) shows the behavior over the entire 1.5-μs pulse. The diode was found to oscillate at 9.7 GHz, the peak output power was 15.8 W, and the diode operating voltage was approximately 100 V. Fig. 5(b) shows that, for the injection-locked case, the diode turns on faster than for the free-running case. (In Figs. 4 and 5, an additional 6-ns delay is introduced in the detected RF waveform relative to the bias-current waveform due to the measurement setup.)

Table I shows the experimental results for the injection-locked case as the injection signal power is varied. The injection frequency was 10 GHz and the (peak) bias current was $I_b=0.84$ A, or $J_{dc}=646$ A/cm^2. P_{RF} is the (peak) RF power generated by the IMPATT and does not include the power delivered by the injection source P_{in}. T_j is the average junction temperature calculated from the experimentally determined thermal resistance. It was found experimentally that if the injection power was reduced below 2 W, the IMPATT did not lock with the injection source.

The thermal resistance was experimentally determined to be $R_{th}=5$°K/W for the diode and 1°K/W for the mount. Since the temperature in the mount changes more slowly than the diode temperature [6], the 1°K/W contribution was assumed to increase the ambient temperature, T_A in (4), from room temperature as follows:

$$T_A=300\text{°K}+64.7\text{ W}\times0.45\times1\text{° K/W}=329\text{°K} \tag{5}$$

where 64.7 W is the peak dissipated power in the diode and 0.45

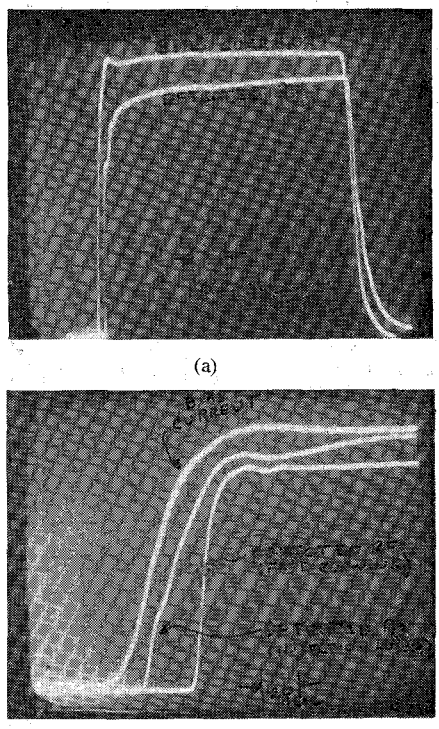

(a)

(b)

Fig. 5. (a) Bias current and RF power for the free-running case and (b) comparison between free-running and injection-locked turn-on characteristics (f_0 = injection frequency = 10 GHz).

TABLE I
INJECTION-LOCKED RESULTS OBSERVED EXPERIMENTALLY AS A FUNCTION OF INJECTED POWER

P_{in} (W, peak)	P_{RF} Added (W, peak)	Average T_J (°K)	Efficiency (%)	V_{dc} (V)
2.00	14.77	479.2	17.9	98.0
2.50	16.28	472.8	20.0	97.0
3.00	17.44	472.0	21.2	98.0
3.50	17.63	471.4	21.4	98.0
3.75	17.39	472.1	21.1	98.0
4.00	16.51	474.5	20.1	98.0
4.50	16.12	475.6	19.6	98.0
5.00	15.88	476.2	19.3	98.0

$f_0 = 10$ GHz, $J_{dc} = 646$ A/cm^2, pulse width = 1.5 μs and duty factor = 45 percent.

is the duty factor. The IMPATT diodes were fabricated in a quad mesa structure; an appropriate thermal relaxation time for this arrangement is $\tau = 8$ μs in (4). Using these values, (4) implies that, in order for the average diode temperature to be 473°K (see Table I), the diode temperature at the beginning of the bias current pulse must be approximately 460°K in the steady state.

Fig. 6(a) shows the start-up behavior obtained from the quasi-static simulation for the free-running case. For comparison, the corresponding portion of the experimentally observed RF power from Fig. 4(a) is also shown. The amplitude of the experimental curve is normalized so that both the experimental and theoretical curves reach the same maximum RF power level. The bias current increases linearly from zero at $t = 0$ to $J_{dc} = 646$ A/cm^2

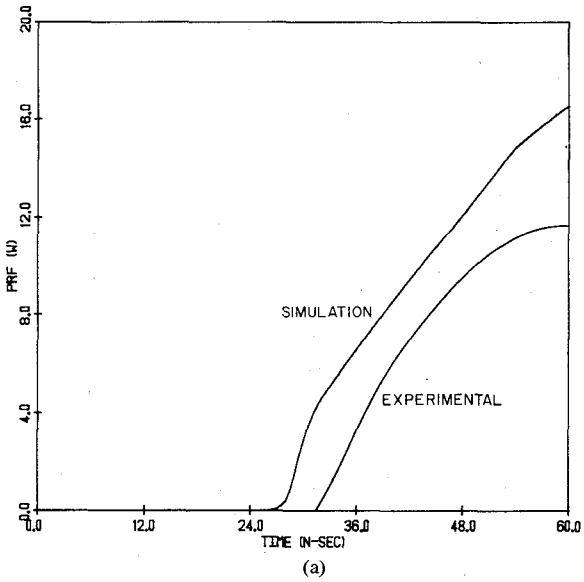

(a)

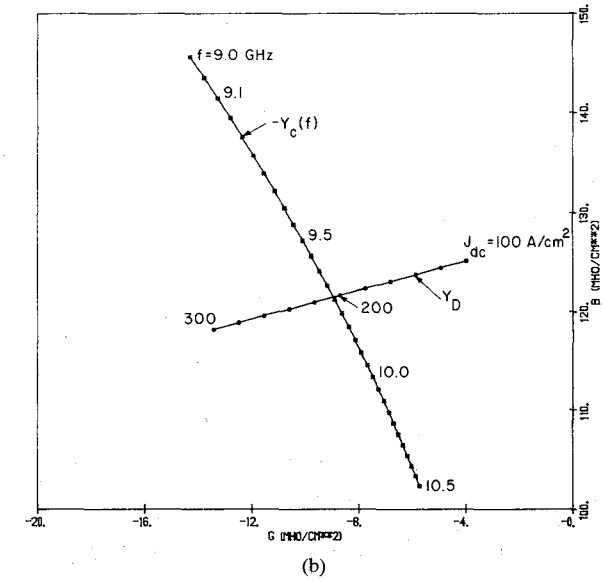

(b)

Fig. 6. (a) Start-up behavior for the free-running simulation ($J_{dc}(t = 0) = 0$, $J_{dc}(t = 60$ ns$) = 646$ A/cm^2, $T(0) = 460°$ K and $\tau = 8$ μs) and (b) admittance plot of $Y_D(V_{RF} = 0, T = 460°$ K; $J_{dc})$ and $-Y_c$(f).

at $t = 60$ ns in Fig. 6(a). The starting temperature at $t = 0$ is 460°K. From Fig. 4(a), the detected RF power turns on approximately 32 ns after the bias current begins to increase (recall the additional 6-ns delay in the measurement system); this experimental delay is very close to the delay resulting from the simulation in Fig. 6(a). Fig. 6(b) shows a plot of the circuit admittance versus real frequency ($\sigma = 0$) and small-signal device admittance versus J_{dc} at the starting temperature $T = 460$°K. From (2), V_{RF} will not increase until (1) is satisfied for a value of s such that $\mathrm{Re}\{s\} = \sigma > 0$. In Fig. 6(b), the region to the right of the $-Y_c(f)$ curve corresponds to $-Y_c(s)$ values such that $\mathrm{Re}\{s\} < 0$, and the area to the left of the $-Y_c(f)$ curve contains $-Y_c(s)$ values such that $\mathrm{Re}\{s\} > 0$. As J_{dc} increases from zero to 200 A/cm^2, the Y_D and $-Y_c(s)$ curves cross for $\sigma < 0$ values and V_{RF} cannot increase. As J_{dc} increases further, the Y_D curve enters the $\sigma > 0$ region and V_{RF} begins to build up. From Fig. 6(b), it is seen that the oscillation frequency will start at approximately 9.7 GHz, which is the experimentally observed frequency for the free-running case.

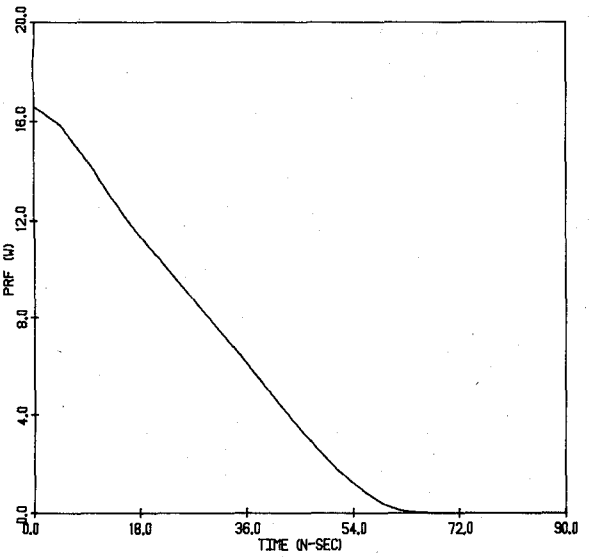

Fig. 7. Turn-off characteristic for the free-running case ($J_{dc}(t=0)=646$ A/cm^2, $J_{dc}(t=90$ ns$)=0$ and $\tau=8$ μs).

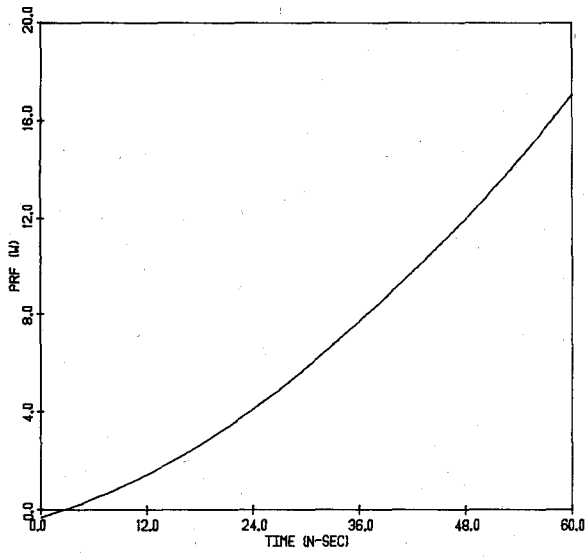

Fig. 8. RF power for the injection-locked start-up transient ($J_{dc}(t=0)=0$, $J_{dc}(t=60$ ns$)=646$ A/cm^2, $\tau=8$ μs, $I_L=0.557$ A, $P_{in}=4.0$ W and $f_0=10$ GHz).

Fig. 7 shows the RF power simulated during the oscillator turnoff where it is assumed that J_{dc} decreases linearly from 646 A/cm^2 at $t=0$ to zero at $t=90$ ns. This result should be compared with Fig. 4(b), although in the experiment J_{dc} departs from the linear waveform.

Fig. 8 shows the start-up transient for the injection-locked case, with $I_l=0.557$ A (see (1) and Fig. 3(a)) so that the incident power from the locking source is $I_l^2/8G_c=4$ W at 10 GHz. Comparison of Fig. 8 with Fig. 6(a) shows that the RF power turns on faster for the injection-locked case than for the free-running case. This is in agreement with the experimental result shown in Fig. 5(b). This is because there is a substantial RF voltage across the diode at $t=0$ due to the injection source.

Table II presents the simulation results as the injection power is varied from 2.0 to 6.0 W. Comparison with Table I shows that the same general RF power variation as observed experimentally is predicted by the simulation, although the simulation predicts a power maximum at $P_{in}=4.0$ W instead of 3.5 W, and the maximum power predicted by the simulation is 16.56 W instead of 17.63 W.

TABLE II
RESULTS OF THE QUASI-STATIC SIMULATION FOR THE INJECTION-LOCKED CASE

I_L (A)	P_{in} (W)	P_{RF} (W, peak)
0.394	2.0	15.50
0.4406	2.5	16.30
0.483	3.0	16.41
0.521	3.5	16.53
0.557	4.0	16.56
0.591	4.5	16.34
0.623	5.0	16.11
0.653	5.5	15.87
0.683	6.0	15.56

$J_{dc}=646$ A/cm^2, $\tau=8$ μs, $f_0=10$ GHz, pulse width $=1.5$ μs, and duty factor $=45$ percent. P_{RF} is averaged over the pulse width.

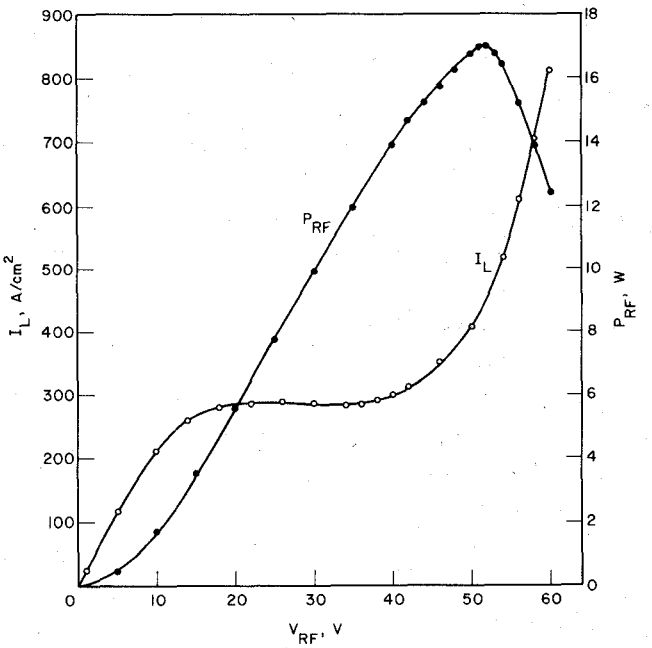

Fig. 9. Locking-signal amplitude and generated RF power versus V_{RF} according to (6) and (7) ($f_0=10$ GHz, $J_{dc}=646$ A/cm^2, $A=1.3\times10^{-3}$ cm^2 and $T=460°$ K).

The behavior indicated in Table II can be understood by examining the curves in Fig. 9. Since, for injection-locking, (1) must be satisfied, the magnitude of the injection current source I_L must satisfy the following relation at the start of the pulse (after the bias current has reached its maximum value):

$$I_L = V_{RF}|Y_c(f=10\text{ GHz}) + Y_D(T=460°\text{ K}, J_{dc}=646\text{ A/cm}^2; V_{RF})|. \quad (6)$$

V_{RF} (the magnitude of the RF voltage at the diode terminals) and the corresponding $Y_D(V_{RF})$ were previously obtained by the diode characterization process, using the steady-state IMPATT simulation program. Equation (6) matches each V_{RF} value with a corresponding I_L for steady-state locking. Also, for each V_{RF}, the

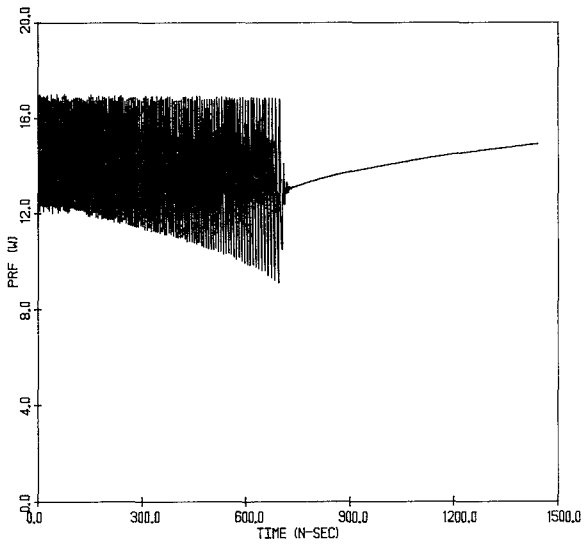

Fig. 10. RF power for the injection-locked case ($J_{dc} = 646$ A/cm^2, $\tau = 8$ μs, $I_L = 0.341$ A, $P_{in} = 1.5$ W and $f_0 = 10$ GHz).

RF power generated by the diode is

$$P_{RF} = -\tfrac{1}{2} G_D V_{RF}^2 \tag{7}$$

where $G_D = \mathrm{Re}\{Y_D(V_{RF})\}$. The expressions in (6) and (7) are plotted in Fig. 9. It is seen that as I_L is varied from 300 A/cm^2 (0.39 A) to 800 A/cm^2 (1.04 A), the RF power first increases, reaches a maximum for $I_L = 450$ A/cm^2 (0.585 A), and then decreases. (P_{RF} in Fig. 9 is the RF power at the start of the pulse, whereas the RF power in Table II is the average over the 1.5-μs pulse width.) Below $I_L \cong 285$ A/cm^2 (0.370 A, $P_{in} = 1.76$ W), it is anticipated from Fig. 9 that locking cannot occur except perhaps at very low P_{RF} values. (It must also be investigated whether the operating points in Fig. 9 are stable.) This expectation is borne out by the simulation in Fig. 10 for which $P_{in} = 1.5$ W ($I_L = 0.341$ A). The diode does not lock until it has heated up to 477°K, so that the curves in Fig. 9 are no longer applicable. As the diode continues to heat up, the generated RF power gradually increases to 14.9 W. This behavior is consistent with the experimental results, since for P_{in} much below 2 W the locking at 10 GHz was not found to be stable.

VI. Conclusions

It has been shown that a large-signal IMPATT diode simulation program employing the drift-diffusion approximation in conjunction with a quasi-static transient simulation can accurately predict experimentally observed behavior at 10 GHz, both for the free-running and injection-locked cases. These programs may be used for diode and circuit design at higher frequencies where measurements become more difficult. However, it may be necessary to include relaxation effects in the IMPATT diode simulation since it has been shown that these effects become significant at low millimeter-wave frequencies [7].

References

[1] K. Kurokawa, "Injection locking of microwave solid-state oscillators," *Proc. IEEE*, vol. 61, pp 1386–1410, Oct 1973.

[2] R. K. Mains, G I. Haddad, and D. F. Peterson, "Simulation of pulsed IMPATT oscillators and injection-locked amplifiers," Tech. Report No. AFWAL-TR-81-1177, Electron Physics Laboratory, University of Michigan, Ann Arbor, Feb. 1981.

[3] P. E. Bauhahn and G. I. Haddad, "IMPATT device simulation and properties," *IEEE Trans. Electron Devices*, vol. ED-24, pp. 634–642, June 1977.

[4] P. E. Bauhahn, "Properties of semiconductor materials and microwave transit-time devices," Ph.D. dissertation, University of Michigan, Ann Arbor, Oct. 1977.

[5] R. K. Mains and G. I. Haddad, "Properties of high-efficiency X-band GaAs IMPATT diodes," Tech. Report No. AFWAL-TR-81-1066, Electron Physics Laboratory, University of Michigan, Ann Arbor, June 1981.

[6] L. H Holway, Jr., "Transient temperature behavior in pulsed double-drift IMPATT diodes," *IEEE Trans. Electron Devices*, vol. ED-27, pp. 433–442, Feb. 1980.

[7] R. K Mains and G. I. Haddad, "Simulation of GaAs IMPATT diodes including energy and velocity transport equations," in *1983 WOCSEMMAD Conf.*, (San Antonio, TX), Feb 1983.

Spectral Domain Analysis of an Elliptic Microstrip Ring Resonator

ARVIND K. SHARMA, MEMBER, IEEE

***Abstract*—The quasi-static capacitance of an elliptic microstrip ring resonator is evaluated with the spectral domain technique. The effect of fringing of fields associated with the structure is determined using this capacitance value in terms of the effective eccentricities of the inner and outer ellipses, the effective values of the ratio of the semimajor and semiminor axes, and the effective dielectric constant. The resonant frequency of the even TM_{c110} mode, calculated utilizing them, is in good agreement with the experiment. Mode charts for the dominant and higher order even and odd TM_{cm10} resonance modes are also presented.**

I. Introduction

Of the various microstrip resonant structures, those with simple geometrical shapes have emerged as the most popular resonant structures in practice. Rectangular, circular disk, and ring resonators, therefore, find extensive applications in oscillators, filters, and circulators. On the other hand, microstrip resonant structures of complex geometrical shapes have not received much attention to date. This mainly is due to inadequate design information available in the literature.

The resonant structures of complex geometrical shapes, in general, provide better performance and greater flexibility in the design. This has been demonstrated for the equilateral triangular microstrip element and the regular hexagonal element in filter and circulator applications [1]–[3]. Although some preliminary results are available, they must be analyzed in greater detail so that they can be meaningfully incorporated into the design of MIC components. With this objective in mind, several different geometrical shapes have recently been investigated in detail [2]–[6].

The elliptic microstrip disk and ring resonators have the potential for being used in practical microwave integrated circuits. The elliptic microstrip disk [6]–[8] can be utilized in harmonic multipliers and parametric amplifiers, since there exists a harmonic relationship between mode frequencies. It also can be used as an antenna element to achieve circular polarization [9]. The elliptic

Manuscript received July 13, 1983; revised September 19, 1983

The author is with the Microwave Technology Center, RCA Laboratories, David Sarnoff Research Center, Princeton, NJ 08540.

0018-9480/84/0200-0212$01.00 ©1984 IEEE